COMPARISON AND ERROR ANALYSIS OF RECONSTRUCTED SWE TO AIRBORNE SNOW OBSERVATORY MEASUREMENTS IN THE UPPER TUOLUMNE BASIN, CA

Edward H. Bair [1,2], Karl Rittger[3,2], Jeff Dozier[4] and Robert E. Davis[1]

ABSTRACT

We present scientific and computing improvements to our new reconstruction model compared to a previous model. Snow water equivalent (SWE) reconstruction involves building a snowpack up in reverse, from melt out to peak SWE, given estimates of melt energy and fractional snow covered area (fSCA). The model was initially tested at an energy balance site on Mammoth Mountain, near the Upper Tuolumne basin, where nearly all the output could be verified and the disappearance of snow was known precisely. A full energy balance version of the model, that computes melt hourly, accurately estimated SWE and most energy balance terms. We were not able to verify a key parameter, the snow albedo, possibly because of low snow depths that affected our ability to measure solar radiation reflected by the snow. A net radiation/degree-day version of the model, that computes melt daily, underestimated SWE, probably because of its coarse daily time step. We then used SWE from the Airborne Snow Observatory (ASO) in 2014 as ground truth to verify the energy balance reconstruction model. Given the high spatial and spectral resolution of ASO measurements, we assume they are an accurate ground truth. Compared to the Snow Data Assimilation System (SNODAS) and the Advanced Microwave Radiometer 2 (AMSR2), reconstruction (with two different fSCA inputs) was by far the most accurate, with a bias of 36-40 mm at the basin wide maximum SWE, and an RMSE of 32-43 mm for all ASO measurement dates. The AMSR2 SWE estimates were generally too low, probably because of deep snow and interference from the canopy. SNODAS tended to overestimate SWE, perhaps because of an overreliance on measurements from snow pillows which are purposely located at heavy snow sites. Finally, we tested the reconstruction model over snow pillows located across the entire Sierra in 2014. The bias was 3 mm and the RMSE 140 mm at the maximum SWE accumulation, showing significant lower than a previous model. (KEYWORDS: reconstruction, Airborne Snow Observatory, Sierra Nevada)

INTRODUCTION

Snow water equivalent (SWE) reconstruction (Martinec and Rango, 1981) involves building a snowpack up in reverse, from melt out to peak SWE, given estimates of melt energy and fractional snow covered area (fSCA). Reconstruction has SWE in large basins in mountain ranges including: the Rocky Mountains (Molotch, 2009), the Hindu Kush (Bair et al., 2014), and the Sierra Nevada (Rittger, 2012; Rittger and Dozier, submitted). The main advantage of reconstruction is that it provides spatially resolved SWE estimates without the need for extensive ground based observations. The biggest disadvantages are that reconstruction can only be run retroactively after snow disappears, and that it is only suitable for areas with little accumulation during the melt season.

The Airborne Snow Observatory (aso.jpl.nasa.gov) is a new project that attempts to provide the most accurate basin wide estimates of SWE to date using a plane with a LiDAR and a spectrometer. Snow depth is measured using the difference between snow covered and dry land LiDAR scans. Snow cover and albedo are concurrently measured using a spectrometer. Using modeled and manually measured snow density, SWE is modeled for the basin. Currently, ASO provides snow albedo (0.365-1.05 μm) and SWE for 2014 and 2015 for the Upper Tuolumne basin at 50 m resolution on their website.

Paper presented Western Snow Conference 2015
[1] US Army Corps of Engineers Cold Regions Research and Engineering Laboratory, Hanover, NH
[2] Earth Research Institute, University of California, Santa Barbara, nbair@eri.ucsb.edu
[3] National Snow and Ice Data Center, Boulder, CO
[4] Bren School of Environmental Science and Management, University of California, Santa Barbara

An outline of this paper is: 1) we describe the three study areas; 2) we present a new reconstruction model with scientific and computing improvements; 3) we test the model at a site with a full suite of energy balance measurements and a precisely known date of maximum SWE and disappearance of snow; 4) we then test the model over the Upper Tuolumne basin, using ASO SWE as ground truth, and compare results with two other operational SWE products; 4) finally, we test the model over the entire Sierra Nevada, using snow pillows for verification.

STUDY AREAS

Figure 1. The Upper Tuolumne basin is shown in red. The University of California – Santa Barbara and Cold Regions Research and Engineering Laboratory Energy Site (CUES) is labeled.

The Sierra Nevada Mountains

The Sierra Nevada (Figure 1) are a 650 km long mountain range that stretch from just south of Lassen Peak in the north to Tehachapi Pass in the south.

The Upper Tuolumne Basin

The Upper Tuolumne (Figure 1 in red) is a small (1,182 km^2) basin in Yosemite National Park. The elevation range is 1102-1387 m. Runoff is primarily from snowmelt and feeds the Hetch Hetchy Reservoir which provides municipal water for 2.4 million people (Bay Area Water Supply & Conservation Agency, 2015).

CUES

The University of California – Santa Barbara and Cold Regions Research and Engineering Laboratory Energy Site (labeled CUES in Figure 1) is a sub-alpine site on Mammoth Mountain, CA at 2940 m. It is 24 km southeast of the Lyell glacier, the highest and most southern point in the Upper Tuolumne basin.

THE RECONSTRUCTION METHOD

Reconstruction (Martinec and Rango, 1981) models the energy required to melt a snowpack. For each pixel, from the time of peak SWE through the disappearance of snow in a satellite image, reconstruction retrospectively builds the snow cover by calculating the amount of snow melted at each time step *j*:

$$SWE_n = \sum_{j=1}^{n} M_j \quad [1]$$

SWE_n and SWE_0 are the SWE at times n and 0, and M_j is the melted SWE. Knowing the value of n when $SWE_n = 0$ (i.e. when fSCA = 0) allows the back-calculation of the initial SWE_0, assuming there is no significant accumulation during the melt. For instance, in the Sierra Nevada, the date of SWE_0 can be computed by interpolating the peak SWE date for each year from snow pillow measurements (Rittger, 2012). Melted SWE is the product of the potential melt $M_{P,j}$ and the fractional snowcover fSCA :

$$M_j = fSCA \times M_{p,j} \quad [2]$$

We used fSCA from two sources, a proprietary product (MODSCAG, Painter et al., 2009) and a publicly available product (MOD10A1, Hall et al., 2006). Both were smoothed, MODSCAG using a time-space method that places less weight on off angle images (Dozier et al., 2008), and MOD10A1 using a 16-day average (Morriss et al., 2014).

We used two methods to calculate potential melt. The first method is a full energy balance model,

$$M_{p,j} = R_j + H_j + L_j + G_j \quad [3]$$

where R is net radiation, H is sensible heat, L is latent heat, and G is heat flow in/out of the snowpack, all at timestep j, which we've omitted for brevity. We assume the snowpack is melting; therefore it is isothermal and G = 0. Thus, Eq. 3 becomes

$$M_p = R + H + L. \quad [4]$$

The second method uses a net radiation/degree-day model (Brubaker et al., 1996) where H and L are replaced with an empirical degree day relationship

$$M_p = \alpha \bar{R} + \beta \bar{D} \quad [5]$$

where α is 0.26 mm W^{-1} m^2 day^{-1}, $\bar{R}$ is the average net radiation above 0 Wm^{-2}, β is an empirical coefficient, and $\bar{D}$ is the average daily air temperature above 0 ºC. For our study, β was set to 1.5 mm C^{-1} day^{-1} (Brubaker et al., 1996; Molotch and Margulis, 2008).

Net radiation R is modeled as,

$$R = S_{\downarrow}(1 - a) + F_{\downarrow} + F_{\uparrow} \quad [6]$$

where $S_{\downarrow}$ is incoming solar radiation, a is the broadband snow albedo, $F_{\downarrow}$ is incoming longwave radiation, and is $F_{\uparrow}$ is outgoing longwave radiation. The broadband albedo a is computed using inversion of the remotely sensed grain radius and the local solar zenith angle (Gardner and Sharp, 2010). For all models runs, MODSCAG estimates of grain radius were used. This albedo estimates were further reduced by half of the λ_{vis} term from the MODIS Dust and Radiative Forcing in Snow (MODDRFS, Painter et al., 2012) to account for light absorbing impurities,

$$a = a_{clean} - \lambda_{vis}/2 \quad [7]$$

where a_{clean} is the clean snow albedo predicted by the albedo model (i.e. Gardner and Sharp, 2010). The term λ_{vis} is an estimate of the difference between the dirty and the clean snow albedo in the visible spectrum (0.350-0.876 µm), which is where light absorbing impurities have the greatest impact for snow. Since is a is a broadband albedo and about half of the sun's energy is in the visible spectrum, we use half of the λ_{vis} estimate.

All of the energy balance terms are modeled using downscaled data from the 1/8º North American Land Data Assimilation System Version 2 (NLDAS-2, Xia et al., 2012). The downscaling process involves a bicubic resampling of the 1/8º energy balance data and elevation model to the model scale. In this study, the model scale is 500 m in a California Albers Equal Area projection. For elevation dependent terms, the difference between the model scale DEM,

resampled from Shuttle Radar Topography Mission data (Farr et al., 2007), and the resampled NLDAS-2 DEM was used. Vegetation inputs for the model came from the National Land Cover Database (Homer et al., 2007), resampled to our model scale.

Shortwave

Incoming solar is by separated into beam $B_{\downarrow}$ and diffuse components $D_{\downarrow}$

$$S_{\downarrow} = B_{\downarrow} + D_{\downarrow} \quad [8]$$

using an empirical relationships (Erbs et al., 1982; Olyphant, 1984) based on transmittance T,

$$T = \frac{S_{\downarrow}}{\mu_0 S_0} \quad [9]$$

where μ_0 is the exoatmospheric (unrefracted) solar zenith angle and S_0 is exoatmospheric irradiance. The direct solar radiation is then scaled by elevation z

$$B_{\downarrow}(z) = \mu_{0,r} S_0 e^{-\tau_z m} \quad [10]$$

where $\mu_{0,r}$ is the (refraction corrected) cosine of the solar zenith angle, m is the airmass (Kasten and Young, 1989), and τ_z is the optical depth at elevation z,

$$\tau_z = \frac{P_z}{P}\tau \quad [11]$$

with P the reference (NLDAS-2) atmospheric pressure, P_z the reference pressure (in Pa) adjusted using a standard lapse rate and the elevation difference between the reference and the fine scale elevation model. The optical depth τ is

$$\tau = \frac{-\ln T}{m}. \quad [12]$$

Then, the elevation corrected beam $B_{\downarrow}(z)$ is scaled by the cosine of the local solar zenith angle μ, along with a binary shadowing mask δ computed from local horizon angles (Dozier and Frew, 1990),

$$B_{s\downarrow} = \delta \mu B_{\downarrow}(z). \quad [13]$$

Diffuse radiation is also corrected by elevation using an empirical formula (Dubayah and Loechel, 1997) and scaled by the view factor V_d (Dozier and Frew, 1990),

$$D_{s\downarrow} = D_{\downarrow}(z) V_d. \quad [14]$$

The corrected beam and diffuse radiation are then further adjusted by vegetation transmissivity (Marks et al., 1999; Garen and Marks, 2005).

Instead of using the bias corrected incoming shortwave from NLDAS-2, we used the uncorrected shortwave (NLDAS-2 Forcing B dataset) and performed our own linear bias correction on the direct and diffuse components based on regressions with measurements from CUES during snowmelt in 2014. The bias corrections are:

$$B_{s,c\downarrow} = \alpha_B D_{s\downarrow} + \beta_B \quad [15]$$

and

$$D_{s,c\downarrow} = \alpha_D D_{s\downarrow} + \beta_D \quad [16]$$

where $B_{s,c\downarrow}$ and $D_{s,c\downarrow}$ are the bias corrected beam and diffuse components with $\alpha_B = 0.71$, $\beta_B = -19$, $\alpha_D = 1.39$, and $\beta_D = 6$. Our bias correction better matched ground measurements of direct and diffuse shortwave at CUES than the bias correction from NLDAS-2. We suspect this is due to snow-cloud discrimination issues, which have been shown to cause overestimates in NLDAS shortwave data (Cosgrove et al., 2003; Pinker et al., 2003).

Longwave

Incoming longwave $F_\downarrow$ is modeled as the sum of incoming longwave from the atmosphere $F_{a\downarrow}$ and from surrounding terrain $F_{T\downarrow}$ (Rittger, 2012),

$$F_\downarrow = F_{a\downarrow} + F_{T\downarrow} \quad [17]$$

with

$$F_{a\downarrow} = V_d \varepsilon_A \sigma T_a^4 \quad [18]$$

where ε_A is the atmospheric emissivity downscaled from reference estimates (NLDAS-2), σ is the Steffan-Boltzman constant 5.67×10^{-8} W m^{-2} K^{-4}, and T_a is the air temperature in Kelvin, which like P_z, was computed using a standard lapse rate and the difference between the reference and the fine scale elevation model. Further,

$$F_{T\downarrow} = (1 - V_d)\varepsilon_s \sigma T_s^4 \quad [19]$$

where ε_S is the emissivity of snow, assumed to be 0.99, and T_s is the snow surface temperature, assumed to be the lesser of T_a or 0 ºC. The incoming longwave is then adjusted for vegetation using an empirical approach (Garen and Marks, 2005) based on canopy cover. Outgoing longwave is the sum of the Steffan-Boltzman radiation model for snow and the 1% of incoming radiation that is reflected,

$$F_\uparrow = -\varepsilon_s \sigma T_s^4 + (1 - \varepsilon_s) F_\downarrow \quad [20]$$

Sensible and Latent Heat

Sensible heat H and latent heat L are (Liston, 1995)

$$H = \rho_a C_p D_h \zeta (T_a - T_s) \quad [21]$$

and

$$L = \rho_a L_v D_e \zeta \left(\theta \frac{e_a - e_s}{P_z} \right) \quad [22]$$

where: ρ_a is the density of air; C_p is the specific heat of air; $D_{h,e}$ are exchange coefficients for sensible and latent heat, respectively; ζ is a non-dimensional stability function; $\theta = 0.622$ and $e_{a,s}$ are the vapor pressures of air and ice, respectively. The exchange coefficients $D_{h,e}$ are

$$D_{h,e} = \frac{\kappa^2 u_r}{\left[\ln\left({}^{z_r}/_{z_0}\right)\right]^2} \quad [23]$$

with $\kappa = 0.4$ as Von Karman's constant, u_r as the wind speed at reference height z_r, and z_0 as the roughness height. In this study, z_r= 10 m, based on NLDAS-2 wind speeds, and $z_0 = 0.5$ mm, a reasonable approximation for snow (Brock et al., 2006). Wind speed was downscaled using resampled NLDAS-2 u and v component estimates, adjusted for terrain curvature, wind slope, and vegetation (Liston and Sturm, 1998; Liston et al., 2007). The ice vapor pressure $e_s(T_s)$ is from an empirical approximation (Buck, 1981). The air vapor pressure e_a is given as:

$$e_a = Q \frac{P_z}{\theta} \quad [24]$$

where Q is the specific humidity, downscaled from reference (NLDAS-2) data. For unstable atmospheric conditions ($T_s > T_a$), the stability function ζ is

$$\zeta = 1 - \frac{\eta R_i}{1 + \gamma |R_i|^{1/2}} \quad [25]$$

with R_i as the Richardson number, given by

$$R_i = \frac{g z_r (T_a - T_s)}{T_a u_r^2} \quad [26]$$

where g is gravity and γ is

$$\gamma = \varphi \eta \frac{D_{h,e}}{u_r} \left(\frac{z_r}{z_0}\right)^{1/2} \quad [27]$$

with $\eta = 9.4$ and $\varphi = 5.3$. For stable atmospheric conditions ($T_s < T_a$), the stability function ζ is

$$\zeta = (1 + \eta^* R_i) \quad [28]$$

where $\eta^* = \eta/2$. For neutral conditions ($T_s = T_a$),

$$\zeta = 1 \quad [29]$$

RESULTS AND DISCUSSION

CUES

By running the models at CUES, we were able to eliminate any uncertainty in snow cover since the peak and disappearance of snow was precisely known. In general, the model matched the measurements at the site well (Figure 2), with the exception of wind speed, latent, and sensible heat. These two energy balance components depend on an accurate wind speed estimate. Given the complex nature of wind in the mountains, it's not surprising that the wind speed was poorly modeled. We suggest this scatter is not a significant problem, as latent and sensible heat are usually small relative to net radiation, and nearly cancel each other (Marks and Dozier, 1992). We were not able to verify our snow albedo estimates, as measurements from an albedometer at CUES were consistently too low, e.g. < 0.75 for clean fresh snow. We hypothesize that the low snow depths in 2014 put the downlooking radiometer too far above the snow surface, allowing darker objects, such as trees, to be seen. We are investigating mounting the albedometer on a moveable boom that will keep the radiometers close to the snow surface throughout the snow season.

Likewise, SWE from the full energy balance model matched up well with SWE measured at CUES, both from a snow pillow, and from sensor estimates (Figure 3). The full energy balance model produced more SWE than the Brubaker et al. model. We suggest this is because the Brubaker et al. model computes melt daily while the full energy balance model computes SWE hourly. An analysis (not shown) of both models allowed to produce negative melt values shows that the Brubaker et al. model produces more SWE than the energy balance model. This reversal suggests that the daily melt timestep is responsible for the SWE underestimate in the Brubaker et al. model. In other words, it is the small number of hourly positive melt values in the energy balance model that cause it to produce more SWE.

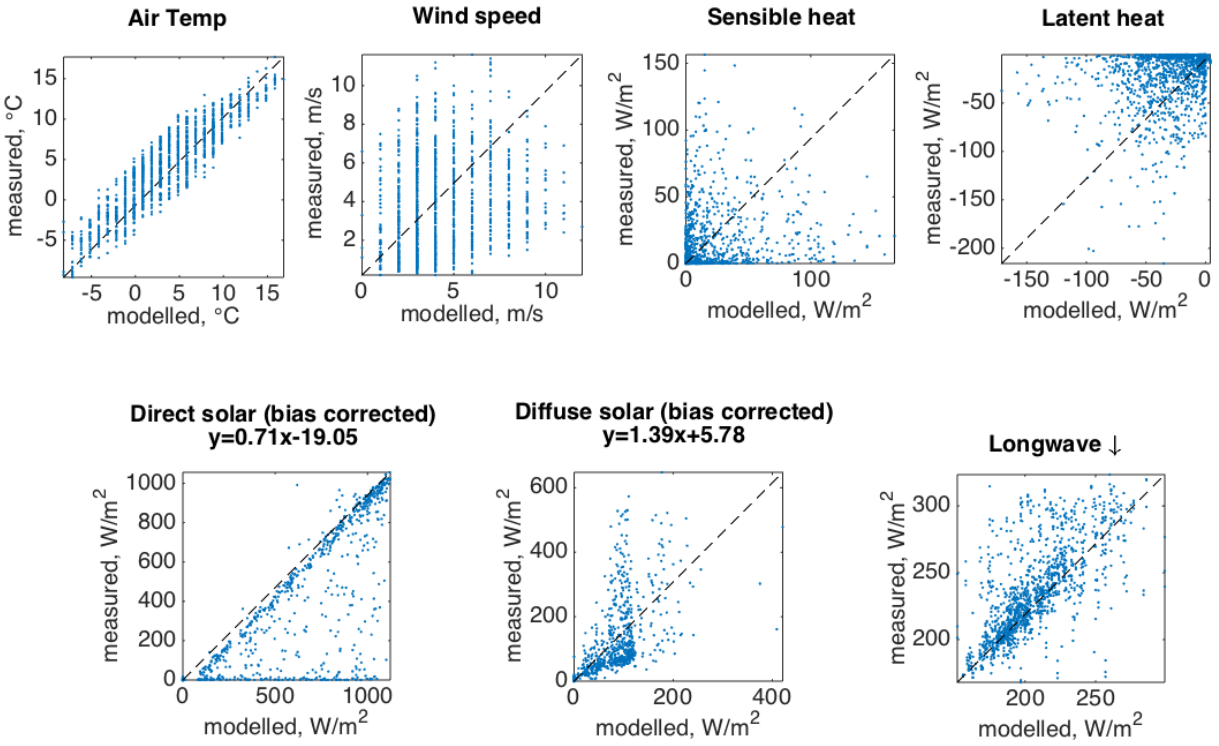

Figure 2. Hourly energy balance components compared to CUES, 4/10-5/30/14.

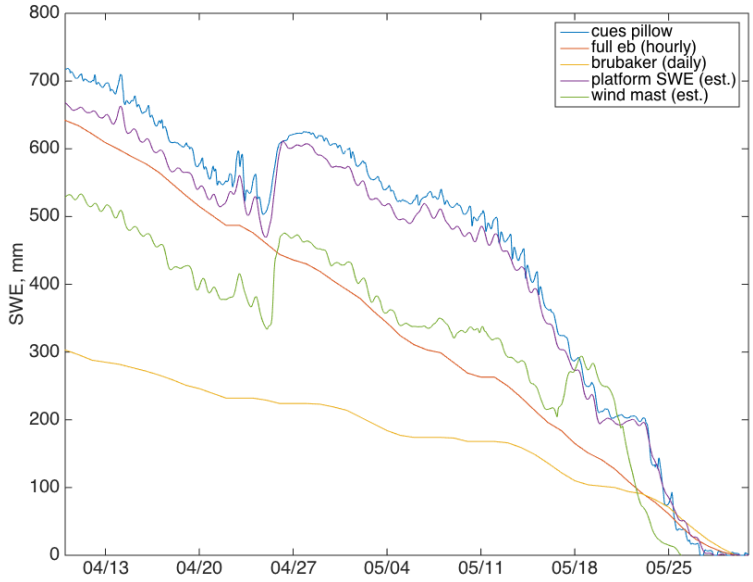

Figure 3. SWE measurements and estimates at CUES, 4/10-5/30/14. The measurement is from a snow pillow ("cues pillow"). The "full eb" model refers to SWE from the full energy balance reconstruction model, while the "brubaker" model refers the SWE from the net radiation/degree-day model. The "platform" and "wind mast" with the "(est.)" suffix are SWE estimates based on density measured at the pillow and depth from ultrasonic pingers at different locations.

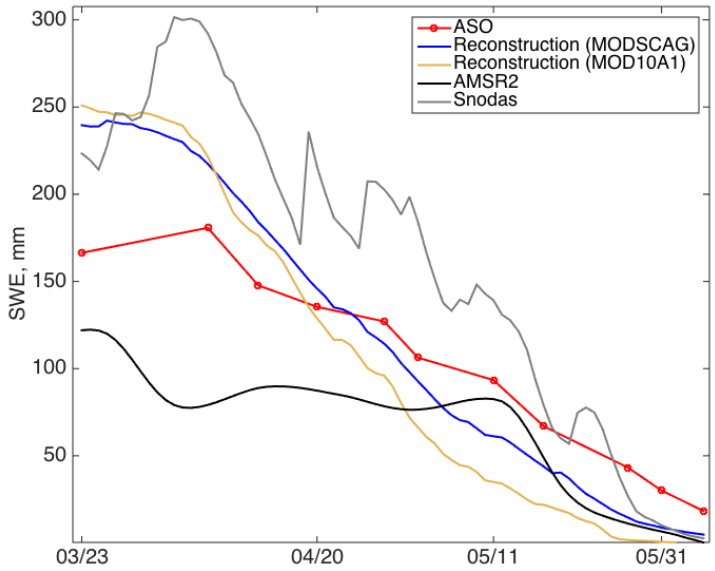

Figure 4. Basin wide average SWE from three different products compared to ASO SWE measurement for the Upper Tuolumne Basin in 2014. AMSR2 is a satellite based operational passive microwave product (Kelly, 2013). Snodas (Snow Data Assimilation System, National Operational Hydrologic Remote Sensing Center, 2004) is an operational SWE product that uses ground and satellite measurements.

Upper Tuolumne

Compared to ASO basin wide SWE measurements, reconstruction performed far better than any other product, with scant difference between models run with different fSCA inputs (MODSCAG or MOD10A1 in Figure 4 and Table 1). At the peak (4/7/14), reconstruction overestimates SWE, but only slightly. Later in the season, reconstruction underestimates SWE, with a worse miss using MOD10A1 compared to MODSCAG. Examining the spatial distribution of SWE throughout the melt season (Figure 5), we suggest these underestimates are due to failures to detect shallow snow. This is a known problem with snow detection as thin snowpacks substantially darken because of transmission of light to the underlying ground. For melting snow, Warren and Wiscombe (1980) estimate that a snowpack becomes optically finite at 200 mm SWE. In addition, the Lidar used for ASO measurements is only accurate to 100 mm in depth. Assuming the snow is 50% water during melt, this suggests a 50 mm shallow depth mapping threshold for ASO measurements.

Whole Sierra

Last, we tested the model (using MODSCAG fSCA) against pillow measurements across the Sierra in 2014 (Figure 6). The bias was only 3 mm and the RMSE was 140 mm. This compares with a previous version of the model

	For peak SWE on 4/7/14		For all ASO dates
Method	**Mean SWE, mm**	**Bias, mm**	**RMSE, mm**
ASO	181	0	0
Reconstruction (MODSCAG)	217	36	32
Reconstruction (MOD10A1)	221	40	43
AMSR2	79	-102	46
Snodas	292	111	64

Table 1. Error analysis for several SWE products compared to ASO measurements. The bias is ASO SWE subtracted from the SWE estimate. RMSE is root mean squared error.

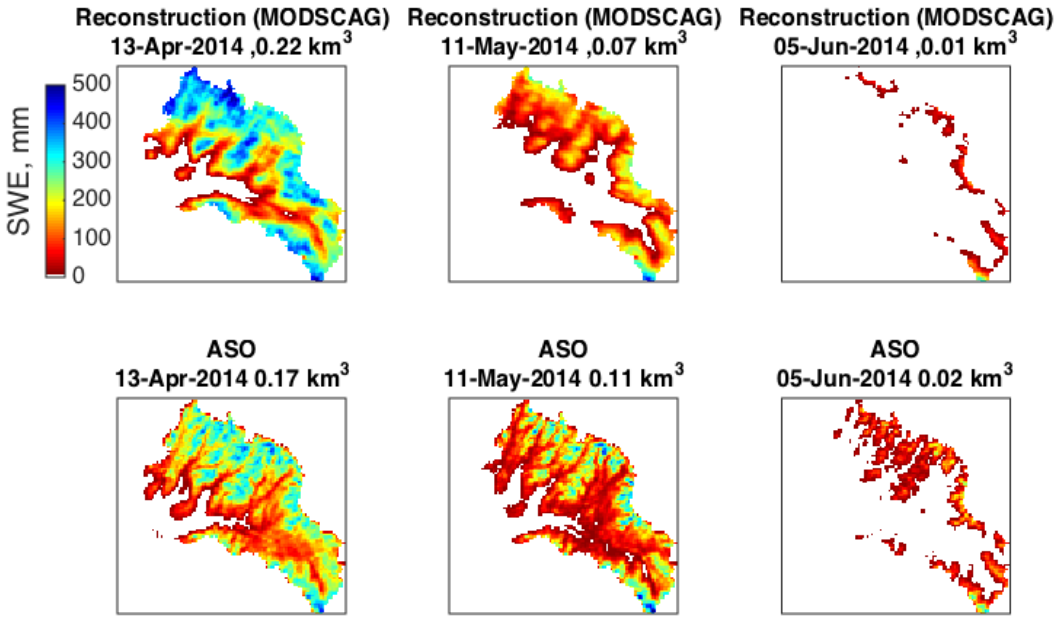

Figure 5. ASO and reconstructed SWE in the Upper Tuolumne.

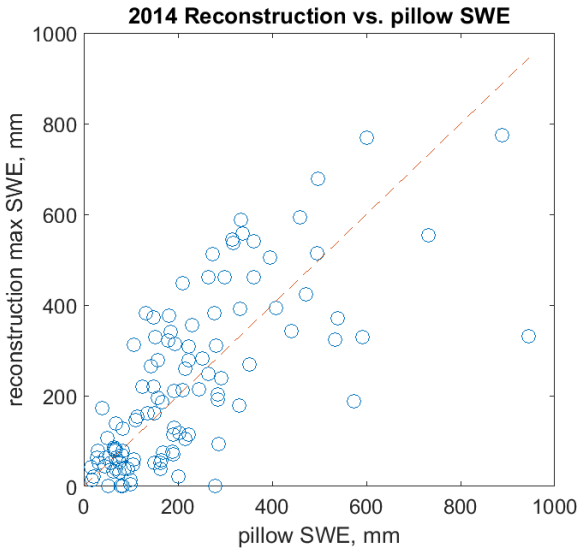

Figure 6. Reconstruction verification using maximum SWE accumulation at snow pillows for 2014. N=104 snow pillows. A 1:1 line is shown in red. The bias is 3 mm and the RMSE is 140 mm.

(Rittger, 2012), which was evaluated similarly, but over a longer period (2000-2011). In that model, the bias was 38 mm and the RMSE was 249 mm.

CONCLUSION

We presented a new SWE reconstruction model and compared it to other models and products. Our model reconstructed energy balance components and SWE accurately at a sub-alpine test site with precisely known snow peak and disappearance. We were not able to validate snow albedo, a key input in any snow melt model, but plan on doing so in the future. Using ASO SWE measurements in the Upper Tuolumne from 2014 as ground truth, our model was the most accurate compared to two other operational products. Last, our model accurately reconstructed SWE across the

Sierra in 2014, using snow pillows for verification. We will also run our model for additional years, including 2015, the driest snow year on record for California, as soon as the snow completely melts out, which should be very shortly.

REFERENCES

Bair, E.H., Dozier, J., Rittger, K., Vuyovich, C.M. and R.E. Davis. 2014. SWE estimates in Afghanistan and the Sierra Nevada using passive microwave and reconstruction, Western Snow Conference, Durango, CO.

Bay Area Water Supply & Conservation Agency. 2015. Hetch Hetchy Water System.

Brock, B.W., Willis, I.C. and M.J. Sharp. 2006. Measurement and parameterization of aerodynamic roughness length variations at Haut Glacier d'Arolla, Switzerland. Journal of Glaciology, 52(177): 281-297, doi: 10.3189/172756506781828746.

Brubaker, K., Rango, A. and W. Kustas. 1996. Incorporating radiation inputs into the snowmelt runoff model. Hydrological Processes, 10: 1329-1343.

Buck, A.L. 1981. New Equations for Computing Vapor Pressure and Enhancement Factor. Journal of Applied Meteorology, 20(12): 1527-1532, doi: 10.1175/1520-0450(1981)020<1527:NEFCVP>2.0.CO;2.

Cosgrove, B.A., Lohmann, D., Mitchell, K.E., Houser, P.R., Wood, E.F., Schaake, J.C., Robock, A., Marshall, C., Sheffield, J., Duan, Q., Luo, L., Higgins, R.W., Pinker, R.T., Tarpley, J.D. and J. Meng. 2003. Real-time and retrospective forcing in the North American Land Data Assimilation System (NLDAS) project. Journal of Geophysical Research: Atmospheres, 108(D22): n/a-n/a, doi: 10.1029/2002JD003118.

Dozier, J. and J. Frew. 1990. Rapid calculation of terrain parameters for radiation modeling from digital elevation data. IEEE Transactions on Geoscience and Remote Sensing, 28(5): 963-969, doi: 10.1109/36.58986.

Dozier, J., Painter, T.H., Rittger, K. and J.E. Frew. 2008. Time-space continuity of daily maps of fractional snow cover and albedo from MODIS. Advances in Water Resources, 31: 1515-1526, doi: 10.1016/j.advwatres.2008.08.011.

Dubayah, R. and S. Loechel. 1997. Modeling Topographic Solar Radiation Using GOES Data. Journal of Applied Meteorology, 36(2): 141-154, doi: 10.1175/1520-0450(1997)036<0141:MTSRUG>2.0.CO;2.

Erbs, D.G., Klein, S.A. and J.A. Duffie. 1982. Estimation of the diffuse radiation fraction for hourly, daily and monthly-average global radiation. Solar Energy, 28(4): 293-302, doi: 10.1016/0038-092X(82)90302-4.

Farr, T.G., Rosen, P.A., Caro, E., Crippen, R., Duren, R., Hensley, S., Kobrick, M., Paller, M., Rodriguez, E., Roth, L., Seal, D., Shaffer, S., Shimada, J., Umland, J., Werner, M., Oskin, M., Burbank, D. and D. Alsdorf. 2007. The Shuttle Radar Topography Mission. Reviews of Geophysics, 45(2): n/a-n/a, doi: 10.1029/2005RG000183.

Gardner, A.S. and M.J. Sharp. 2010. A review of snow and ice albedo and the development of a new physically based broadband albedo parameterization. Journal of Geophysical Research: Earth Surface, 115(F1): F01009, doi: 10.1029/2009JF001444.

Garen, D.C. and D. Marks. 2005. Spatially distributed energy balance snowmelt modelling in a mountainous river basin: estimation of meteorological inputs and verification of model results. Journal of Hydrology, 315(1–4): 126-153, doi: 10.1016/j.jhydrol.2005.03.026.

Hall, D.K., Salomonson, V.V. and G.A. Riggs. 2006. MODIS/Terra Snow Cover Daily L3 Global 500m Grid, Fractional Snow Covered Area. Boulder, Colorado USA: NASA National Snow and Ice Data Center Distributed Active Archive Center.

Homer, C., J., D., J., F., Coan, M., Hossain, N., Larson, C., Herold, N., McKerrow, A., VanDriel, J.N. and J. Wickham. 2007. Completion of the 2001 National Land Cover Database for the Conterminous United States. Photogrammetric Engineering and Remote Sensing, 73(4): 337-341.

Kasten, F. and A.T. Young. 1989. Revised optical air mass tables and approximation formula. Applied Optics, 28(22): 4735-4738, doi: 10.1364/AO.28.004735.

Kelly, R. 2013. Descriptions of GCOM-W1 AMSR2 Level 1R and Level 2 Algorithms. Earth Observation Research Center, Japan Aerospace Exploration Agency, pp. 17.

Liston, G.E. 1995. Local Advection of Momentum, Heat, and Moisture during the Melt of Patchy Snow Covers. Journal of Applied Meteorology, 34(7): 1705-1715, doi: 10.1175/1520-0450-34.7.1705.

Liston, G.E., Haehnel, R.B., Sturm, M., Hiemstra, C.A., Berezovskaya, S. and R.D. Tabler. 2007. Instruments and methods: Simulating complex snow distributions in windy environments using SnowTran-3D. Journal of Glaciology, 53: 241-256, doi: 10.3189/172756507782202865.

Liston, G.E. and M. Sturm. 1998. A snow-transport model for complex terrain. Journal of Glaciology, 44(148): 498-516.

Marks, D., Domingo, J., Susong, D., Link, T. and D. Garen. 1999. A spatially distributed energy balance snowmelt model for application in mountain basins. Hydrological Processes, 13(12-13): 1935-1959, doi: 10.1002/(SICI)1099-1085(199909)13:12/13<1935::AID-HYP868>3.0.CO;2-C.

Marks, D. and J. Dozier. 1992. Climate and energy exchange at the snow surface in the Alpine Region of the Sierra Nevada: 2. Snow cover energy balance. Water Resources Research, 28(11): 3043-3054, doi: 10.1029/92wr01483.

Martinec, J. and A. Rango. 1981. Areal distribution of snow water equivalent evaluated by snow cover monitoring. Water Resources Research, 17(5): 1480-1488, doi: 10.1029/WR017i005p01480.

Molotch, N.P. 2009. Reconstructing snow water equivalent in the Rio Grande headwaters using remotely sensed snow cover data and a spatially distributed snowmelt model. Hydrological Processes, 23(7): 1076-1089, doi: 10.1002/hyp.7206.

Molotch, N.P. and S.A. Margulis. 2008. Estimating the distribution of snow water equivalent using remotely sensed snow cover data and a spatially distributed snowmelt model: A multi-resolution, multi-sensor comparison. Advances in Water Resources, 31(11): 1503-1514, doi: dx.doi.org/10.1016/j.advwatres.2008.07.017.

Morriss, B.F., Ochs, E., Newman, S.D., Deeb, E.J., Daly, S.F. and J.J. Gagnon. 2014. An operational snow covered area mapping algorithm for MODIS snow products, Eastern Snow Conference and ESC Proceedings, Boone, NC.

National Operational Hydrologic Remote Sensing Center. 2004. Snow Data Assimilation System (SNODAS) Data Products at NSIDC. National Snow and Ice Data Center, Boulder, CO.

Olyphant, G.A. 1984. Insolation Topoclimates and Potential Ablation in Alpine Snow Accumulation Basins: Front Range, Colorado. Water Resources Research, 20(4): 491-498, doi: 10.1029/WR020i004p00491.

Painter, T.H., Bryant, A.C., and S.M. Skiles. 2012. Radiative forcing by light absorbing impurities in snow from MODIS surface reflectance data. Geophysical Research Letters, 39(17): L17502, doi: 10.1029/2012GL052457.

Painter, T.H., Rittger, K., McKenzie, C., Slaughter, P., Davis, R.E. and J. Dozier. 2009. Retrieval of subpixel snow-covered area, grain size, and albedo from MODIS. Remote Sensing of Environment, 113: 868-879, doi: 10.1016/j.rse.2009.01.001.

Pinker, R.T., Tarpley, J.D., Laszlo, I., Mitchell, K.E., Houser, P.R., Wood, E.F., Schaake, J.C., Robock, A., Lohmann, D., Cosgrove, B.A., Sheffield, J., Duan, Q., Luo, L. and R.W. Higgins. 2003. Surface radiation budgets in support of the GEWEX Continental-Scale International Project (GCIP) and the GEWEX Americas Prediction Project (GAPP), including the North American Land Data Assimilation System (NLDAS) project. Journal of Geophysical Research: Atmospheres, 108(D22): n/a-n/a, doi: 10.1029/2002JD003301.

Rittger, K. 2012. Spatial estimates of snow water equivalent in the Sierra Nevada. Ph.D. Thesis, Unversity of California, Santa Barbara, 225 pp.

Rittger, K. and J. Dozier. Submitted. Spatial estimates of snow water equivalent from reconstruction. Advances in Water Resources.

Wiscombe, W.J. and Warren, S.G. 1980. A model for the spectral albedo of snow, I, Pure snow. J. Atmos. Sci., 37(12): 2712-2733, doi: 10.1175/1520-0469(1980)037<2712:AMFTSA>2.0.CO;2.

Xia, Y., Mitchell, K., Ek, M., Sheffield, J., Cosgrove, B., Wood, E., Luo, L., Alonge, C., Wei, H., Meng, J., Livneh, B., Lettenmaier, D., Koren, V., Duan, Q., Mo, K., Fan, Y. and D. Mocko. 2012. Continental-scale water and energy flux analysis and validation for the North American Land Data Assimilation System project phase 2 (NLDAS-2): 1. Intercomparison and application of model products. Journal of Geophysical Research: Atmospheres, 117(D3): n/a-n/a, doi: 10.1029/2011JD016048.